Springer

KSME

Journal of Mechanical Science and Technology 33 (5) (2019) 2267~2279
www.springerlink.com/content/1738-494x(Print)/1976-3824(Online)
DOI 10.1007/s12206-019-0428-5

Free vibration analysis of bi-directional functionally graded annular plates using finite annular prism methods †

Chih-Ping Wu* and Lu-Ting Yu

Department of Civil Engineering, National Cheng Kung University, Tainan 70101, Taiwan

(Manuscript Received August 13, 2018; Revised January 14, 2019; Accepted January 25, 2019)

Abstract

Based on Reissner's mixed variational theorem, the authors develop a finite annular prism method (FAPM) for the three-dimensional (3D) free vibration analysis of bi-directional functionally graded (FG) annular plates with assorted boundary conditions. In this formulation, the FG annular plate is divided into a number of finite annular prisms with triangular cross-sections, in which Fourier functions and Lagrange polynomials are used to interpolate the circumferential direction and radial-thickness surface variations of primary field variables in each individual prism, respectively. The material properties of the FG annular plate are assumed to obey an exponential function distribution varying doubly exponentially through the radial-thickness surface. These FAPM solutions for the frequency parameters and their corresponding mode shapes of the FG annular plate closely agree with the solutions obtained using other 3D approaches available in the literature.

Keywords: Annular plates; Finite annular prism methods; Functionally graded material; Reissner's mixed variation theorem; Various boundary conditions; Vibration

1. Introduction

In recent decades, a new class of materials, the so-called functionally graded materials (FGMs), has been successfully developed and rapidly popularized for use in a variety of advanced industrial fields, such as high performance aircraft, heat engine, armor plating, electronics, and biomedical sectors [1, 2]. In practice, FGMs can be artificially made by mixing two or more different phase materials according to the predefined distributions of the volume fractions of the constituents over the structural domain. Hence, FGM structures have material properties that vary continuously and smoothly over the structural domain, which can be used to avoid interfacial stress concentrations, which often occur in conventional laminated composite structures, the material properties of which suddenly change when they across through the interfaces between adjacent layers. Both the assorted structural analyses of FGM beam-, plate-, and shell-like structures [3-10] and the optimization of the material composition of FGMs to obtain some desired physical properties [11-14], such as natural frequency parameters, critical load parameters, gross stiffness, and total weight, have thus attracted considerable attention. Among these, the review in this work focuses on articles examining the structural behavior of one- and multi-directional functionally graded (FG) annular and circular plates.

A variety of two-dimensional (2D) plate theories for the analysis of conventional laminated composite plates were extended to the analysis of FGM plates, such as the classical plate theory (CPT), first-order shear deformation theory (FSDT), third-order shear deformation theory (TSDT), four-order shear deformation theory (FOSDT), and discrete layer theory. Based on the CPT, Kumar and Lal [15] and Lal and Ahlawat [16] presented analytical and numerical results for the axisymmetric free vibration analysis of bi-directional FG annular and circular plates resting on the Winkler-type foundation either subjected or non-subjected to an initial in-plane load. In conjunction with the FSDT and differential quadrature (DQ) method, Tornabene et al. [17] showed 2D DQ solutions for the vibration analysis of FG conical, cylindrical, and annular plate structures, in which two simple power-law distributions of material properties were assumed, and the issue was also studied by Su et al. [18] using the FSDT combined with the Rayleigh-Ritz method. On the basis of the FSDT and Ritz method, Wang et al. [19] proposed a unified method for the vibration analysis of FG circular, annular, and sector plates with general boundary conditions, in which the material properties of the plate were assumed to obey a general four-parameter power-law distribution through the thickness direction according to the volume fractions of the constituents. The

*Corresponding author. Tel.: +886 6 2757575, Fax.: +886 6 2370804
E-mail address: cpwu@mail.ncku.edu.tw
† Recommended by Associate Editor Heung Soo Kim

material properties of the four-parameter power-law model were also used by Tornabene [20] for the dynamic analysis of moderately thick FG conical shells, cylindrical shells, and annular plates, in which the DQ method was used to discretize the system equations. Based on the FSDT combined with the von Kármán geometrical nonlinearity effect, Amini et al. [21] developed a nonlinear formulation to examine the geometrical nonlinearity effects on the free and forced vibration behavior of FG annular plates. Saidi et al. [22] developed an unconstrained TSDT for the axisymmetric bending and buckling analyses of thick FG circular plates, in which the results of the maximum displacement and critical load parameters of the plates with different values for the volume fractions of the constituents were presented. A TSDT-based finite element method (FEM) was developed by Talha and Singh [23] to investigate both static and free vibration analyses of FGM plates, in which a continuous isoparameter Lagrangian finite element with 13 degrees of freedom per node was used to obtain the corresponding numerical solutions. Hosseini-Hashemi et al. [24] showed the exact closed-form solutions for the natural frequencies of thick circular plates using the TSDT. Sahraee and Saidi [25] investigated the axisymmetric bending behavior of thick FG circular plates using an FOSDT, in which it was found that the maximum values of deflections of the plate obtained using the FOSDT and TSDT were close to each other, while the through-thickness distributions of the shear stress components obtained using the FOSDT were more accurate than those obtained using the TSDT when they were compared with the exact 3D solutions available in the literature. Batra [26] developed a higher-order shear and normal deformable theory for FG incompressible linear elastic plates using the principle of virtual work, and applied it to the free vibration analysis of simply-supported FG rectangular plates. Based on the FSDT and TSDT combined with the meshless method, Ferreira et al. [27] examined the free vibration behavior of FG rectangular plates, in which the Mori-Tanaka technique was used to estimate the effective material properties of these FG plates. Based on a refine theory, Lal and Rani [28] presented analytical and numerical results for the axisymmetric vibration of sandwiched annular plates. Malekzadeh and Hamzehkolaei [29] developed a discrete layer approach combined with the DQ method for the free vibration analysis of multilayered FG annular plates in thermal environment. The above-mentioned 2D advanced and refined plate theories have been included in the Carrier unified formulation (CUF) [30] and can be regarded as its special plate versions.

Some recently proposed numerical methods combined with the 2D refined and advanced plate theories were used for the free vibration analysis of FG plates. Mercan et al. [31] studied the free vibration behavior of FGM and carbon nanotube-reinforced composite annular thick plates using the FSDT and the discrete singular convolution (DSC), in which the regularized Shannon delta kernel and the Lagrange delta sequence kernel were used to discretize the derivatives of the primary variables with respect to the spacial coordinates in terms of linear combinations of their nodal variables. Based on the CST, Shi et al. [32] developed a unified formulation for the free vibration analysis of orthotropic plates of revolution with general boundary conditions, in which the spectro-geometric method and the Rayleigh-Ritz technique were used, such that the geometry of a variety of plates can be described in terms of mathematical or design parameters. An isogeometric finite element approach [33, 34] based on nonuniform rational B-spline (NURBS) basis functions was developed for the free vibration analysis of circular, annular, and sector plates by Qin et al. [35] and that of bi-directional FG plates with variable thickness by Lieu et al. [36]. The NURBS basis functions were used to model the displacement field and geometry of the structures considered, such that they can preserve the exact geometry of the structures and can provide higher continuity of basis functions and their derivatives.

In the above-mentioned 2D refined and advanced plate theories, including the CST, FSDT, TSDT and FOSDT, some kinematic assumptions have to be made *a priori*, and the accuracy of their results are difficult to evaluate when the structural behavior of a very thick plate is investigated because some 3D effects on the plates may not be captured. Development of the 3D analytical and numerical methods for the current issue is thus necessary.

Some three-dimensional (3D) weak- and strong-form formulations have been developed for the assorted structural analyses of one- and multi-directional FG single- and multi-layered plates. Based on the principle of virtual displacements (PVD), So and Leissa [37] and Kang and Leissa [38] developed a weak-form formulation of 3D polynomials-Ritz method to investigate the free vibration behavior of isotropic homogeneous thick circular and annular plates and linearly tapered annular plates, respectively, in which the displacement components were selected as the primary variables, the admissible functions for which were chosen as trigonometric functions in the circumferential coordinate and algebraic polynomials in the radial and thickness coordinates. The 3D Ritz method was also extended to the free vibration analysis of circular and annular plates with different edge conditions by Liew and Yang [39, 40]. The above-mentioned issue was also re-examined by Zhou et al. [41] using a 3D Chebyshev-Ritz method, in which the nominal polynomials were replaced with the Chebyshev polynomials for the admissible functions of the displacement components in the radial and thickness directions, such that a stable numerical operation could be guaranteed even when a large number of admissible functions were used. The 3D Chebyshev-Ritz method was thus extended to the 3D free vibration analysis of isotropic homogeneous thick circular plates on the Pasternak-type foundation by Zhou et al. [42] and to that of FG annular plates in temperature-dependent and -independent environments by Shi and Dong [43] and Dong [44], respectively. Nie and Zhong [45, 46] developed a strong-form formulation of the state space differential quadrature (SSDQ) method for the dynamic analysis of multi-directional FG annular plates with various boundary conditions and simply-supported FG annular sectorial plates. In the SSDQ method, the admissible functions of the displacement components were selected as the harmonic functions in the time domain, Fourier functions in the circumferential coordinate, and DQ interpolation functions in the radial coordinate, such that the 3D motion equations, which comprise a set of partial differential equations, will be reduced as a set of ordinal differential equations in the thickness direction. As a result, the free vibration behavior of the plate can be examined using the state space method. The SSDQ method was also extended to a free vibration analysis of multi-directional FG circular and annular plates by Kermani et al. [47] and Malekzadeh et al. [48]. Vel and Batra [49] presented 3D exact solutions for the free and force vibrations of simply-supported, FG rectangular plates using the power series method. Within the framework of 3D elasticity theory, Zhao et al. [50] presented 3D exact solutions for the free vibration of thick functionally graded annular sector plates with arbitrary boundary conditions. The above-mentioned 3D exact and numerical solutions can provide a reference to assess the performance of a variety of 2D advanced and refined theories.

Most of the 2D refined and advanced plate theories and 3D semi-analytical numerical methods mentioned above were derived on the basis of the PVD, in which the displacement components were regarded as the primary variables, rather than being based on Reissner's mixed variational theorem (RMVT), in which the displacement and transverse stress components were regarded as the primary variables. It is well known that the RMVT-based models are superior to the PVD-based models, especially in the case of laminated composite and multi-layered FGM plates [51-54]. This is mainly due to the fact that the continuity conditions of the displacement and transverse stress components are satisfied at the interfaces between adjacent layers for the former, while only the displacement continuity conditions are satisfied for the latter, that results a set of single-valued solutions of transverse stress components is obtained at the interfaces for the RMVT-based models, while multiple sets of solutions of the transverse stress components are obtained at these places, which violates the 3D elasticity theory. In addition, the highest order of the derivatives of field variables involved in both the strong- and weak-form formulations of the former is one-half lower than that in those of the latter, that results less time consuming required for the RMVT-based models than that required for the PVD-based models.

In order to capture the 3D behavior of FGM plates and shells and overcome the restrictions of 3D analytical methods, such as the complicated solution process and difficulty related to use for one- and multi-directional FGM plates, on the basis of the RMVT, Wu and Li [53, 54] developed the finite rectangular and cylindrical prism methods (FRPM and FCPM) for the analysis of one-directional FG rectangular plates and hollow cylinders, respectively, with various boundary conditions. Wu and Yu [55] developed an isoparametric finite annular

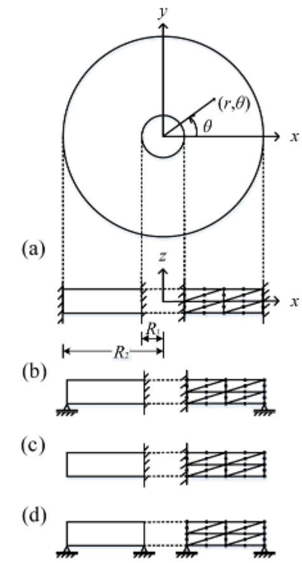

Fig. 1. Configuration and coordinates of an annular plate and the (4x2) mesh of T6 FAPM models with (a) C-C; (b) C-S; (c) C-F; (d) S-S boundary conditions.

prism method (FAPM) with quadrilateral cross-sections for the bending analysis of bi-directional FG circular plates with different boundary conditions. Implementation of these RMVT-based FRPM, FCPM and FAPM proved their solutions to be accurate and to converge rapidly. In the current paper, the FAPM with triangular cross sections is extended to the 3D free vibration analysis of bi-directional FG thick annular plates with combinations of free, clamped, and simply-supported edges. The material properties of the FG annular plates are assumed to obey an exponential function distribution varying doubly exponentially through the radial-thickness surface. A parametric study with regard to some key effects on the natural frequency parameters and the corresponding mode shapes of the bi-directional FG thick annular plates with nine different boundary conditions is undertaken, including the material-property gradient indices, aspect ratios, and different boundary conditions.

2. The isoparametric FAPMs

Consider an N_l-layered bi-directional FG thick annular plate, as shown in Fig. 1, in which N_l is the total number of layers constituting the annular plate. The thickness and mid-surface inner and outer radii of the annular plate are defined as h, R_1 and R_2, respectively. The thickness of each individual layer is $h_m \left(m = 1 - N_l\right)$. The boundary conditions of the annular plate are considered to be combinations of free, clamped and simply-supported edges. The cylindrical global coordinate system (i.e., r, θ and z coordinates) is located on the mid-surface of the annular plate. The typical three-node linear, six-node quadratic and 10-node cubic parent annular prisms in the natural coordinate system are shown in Fig. 2, in which ξ and η denote the natural coordinates, which are located on the right-angle node of the nodal triangular surface of a typical annular prism (i.e., the radial-thickness surface). The mapping relations between the global and natural coordinates of each point in the prism domain are expressed as

$$r^{(e)} = \sum_{i=1}^{n_s} r_i^{(e)} \psi_i^{(e)}(\xi,\eta) \text{ and } z^{(e)} = \sum_{i=1}^{n_s} z_i^{(e)} \psi_i^{(e)}(\xi,\eta) \tag{1}$$

where n_s denotes the degree of approximation used to describe the coordinate transformation for the isoparametric annular prism, and $\psi_i(\xi,\eta)$ $i=1-n_s$ denote the shape (or interpolation) functions of the annular prism. The isoparametric annular prisms are used in the implementation of these FAPMs, in which the degree of approximation used to describe the coordinate transformation is equal to that used to represent each primary field variable, such that the values of n_s are taken to be three, six, and 10 for the linear, quadratic, and cubic FAPM, respectively.

2.1 Kinematic and kinetic assumptions

Since the RMVT is used in this formulation, the displacement and transverse stress components are selected as the primary field variables. Variations of the primary field variables over the radial-thickness nodal surface and circumferential direction are assumed to be separable, and for a typical annular prism of the mth-layer they are thus given by

$$\left[u_r^{(e)}(r,\theta,z,t)\right]^{(m)} = \sum_{i=1}^{n_d}\left[\phi^{(e)}(r,z,t)\right]_i \left[u^{(e)}(\theta)\right]_i^{(m)} \tag{2}$$

$$\left[u_\theta^{(e)}(r,\theta,z,t)\right]^{(m)} = \sum_{i=1}^{n_d}\left[\phi^{(e)}(r,z,t)\right]_i \left[v^{(e)}(\theta)\right]_i^{(m)} \tag{3}$$

$$\left[u_z^{(e)}(r,\theta,z,t)\right]^{(m)} = \sum_{i=1}^{n_d}\left[\phi^{(e)}(r,z,t)\right]_i \left[w^{(e)}(\theta)\right]_i^{(m)} \tag{4}$$

$$\left[\tau_{rz}^{(e)}(r,\theta,z,t)\right]^{(m)} = \sum_{i=1}^{n_d}\left[\phi^{(e)}(r,z,t)\right]_i \left[\tau_{13}^{(e)}(\theta)\right]_i^{(m)} \tag{5}$$

$$\left[\tau_{\theta z}^{(e)}(r,\theta,z,t)\right]^{(m)} = \sum_{i=1}^{n_d}\left[\phi^{(e)}(r,z,t)\right]_i \left[\tau_{23}^{(e)}(\theta)\right]_i^{(m)} \tag{6}$$

$$\left[\sigma_z^{(e)}(r,\theta,z,t)\right]^{(m)} = \sum_{i=1}^{n_d}\left[\phi^{(e)}(r,z,t)\right]_i \left[\sigma_3^{(e)}(\theta)\right]_i^{(m)} \tag{7}$$

where t represents the time variable; $\left(u^{(e)}\right)_i^{(m)}$, $\left(v^{(e)}\right)_i^{(m)}$, $\left(w^{(e)}\right)_i^{(m)}$, $\left(\tau_{13}^{(e)}\right)_i^{(m)}$, $\left(\tau_{23}^{(e)}\right)_i^{(m)}$ and $\left(\sigma_3^{(e)}\right)_i^{(m)}$ with $(i=1, 2, \cdots, n_d)$ are the nodal displacement and transverse stress components of a typical annular prism of the mth-layer of the annular plate, and n_d denotes the total number of nodes of a typical annular prism, such that the values of n_d are three, six, and 10 for the linear, quadratic and cubic annular prisms with triangular cross sections, respectively. The symbols, T3, T6 and T10, are used to represent three-node linear, six-node quadratic, and 10-node cubic annular prisms, the typical parent annular prisms of which in natural coordinates are shown in Fig. 2.

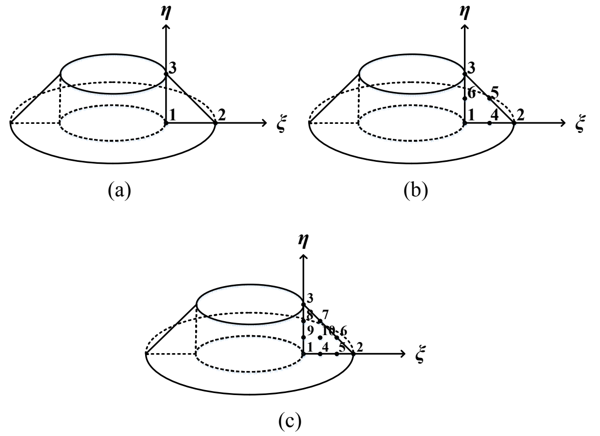

Fig. 2. The FAPM in the natural coordinates: (a) T3 linear prism; (b) T6 quadratic prism; (c) T10 cubic prism.

$\left(\phi^{(e)}\right)_i^{(m)}$ $(i=1,\cdots,n_d)$ are the corresponding shape (or interpolation) functions used to interpolate the primary field variables over the nodal surface of the prism domain.

The linear constitutive equations of the mth-layer, which are valid for the orthotropic materials, are given as

$$\begin{Bmatrix} \sigma_r^{(m)} \\ \sigma_\theta^{(m)} \\ \sigma_z^{(m)} \\ \tau_{\theta z}^{(m)} \\ \tau_{rz}^{(m)} \\ \tau_{r\theta}^{(m)} \end{Bmatrix} = \begin{bmatrix} c_{11}^{(m)} & c_{12}^{(m)} & c_{13}^{(m)} & 0 & 0 & 0 \\ c_{12}^{(m)} & c_{22}^{(m)} & c_{23}^{(m)} & 0 & 0 & 0 \\ c_{13}^{(m)} & c_{23}^{(m)} & c_{33}^{(m)} & 0 & 0 & 0 \\ 0 & 0 & 0 & c_{44}^{(m)} & 0 & 0 \\ 0 & 0 & 0 & 0 & c_{55}^{(m)} & 0 \\ 0 & 0 & 0 & 0 & 0 & c_{66}^{(m)} \end{bmatrix} \begin{Bmatrix} \varepsilon_r^{(m)} \\ \varepsilon_\theta^{(m)} \\ \varepsilon_z^{(m)} \\ \gamma_{\theta z}^{(m)} \\ \gamma_{rz}^{(m)} \\ \gamma_{r\theta}^{(m)} \end{Bmatrix} \tag{8}$$

where $\sigma_r^{(m)}$, $\sigma_\theta^{(m)}, \cdots$ and $\tau_{r\theta}^{(m)}$ are the stress components; $\varepsilon_r^{(m)}$, $\varepsilon_\theta^{(m)}, \cdots$ and $\gamma_{r\theta}^{(m)}$ are the strain components, and $c_{ij}^{(m)}$ are the elastic coefficients, which are considered to be independent of the circumferential coordinate in the analysis, while they are variable over the radial-thickness surface of the annular prism (i.e., $c_{ij}^{(m)}(r,\ z)$).

The strain-displacement relations for a typical annular prism of the mth-layer, based on the assumed displacement components in Eqs. (2)-(4), are given by

$$\left[\varepsilon_r^{(e)}(r,\ \theta,\ z,\ t)\right]^{(m)} = \sum_{i=1}^{n_d}\left(D_r\,\phi_i^{(e)}\right)\left(u_i^{(e)}\right)^{(m)} \tag{9}$$

$$\left[\varepsilon_\theta^{(e)}(r,\theta,z,t)\right]^{(m)} = (1/r)\sum_{i=1}^{n_d}\left(\phi_i^{(e)}\right)\left(v_{i,\theta}^{(e)}\right)^{(m)} + (1/r)\sum_{i=1}^{n_d}\left(\phi_i^{(e)}\right)\left(u_i^{(e)}\right)^{(m)} \tag{10}$$

$$\left[\varepsilon_z^{(e)}(r,\ \theta,\ z,\ t)\right]^{(m)} = \sum_{i=1}^{n_d}\left(D_z\,\phi_i^{(e)}\right)\left(w_i^{(e)}\right)^{(m)} \tag{11}$$

$$\left[\gamma_{rz}^{(e)}(r,\ \theta,\ z,\ t)\right]^{(m)} = \sum_{i=1}^{n_d}\left(D_z\,\phi_i^{(e)}\right)\left(u_i^{(e)}\right)^{(m)} + \sum_{i=1}^{n_d}\left(D_r\,\phi_i^{(e)}\right)\left(w_i^{(e)}\right)^{(m)} \tag{12}$$

$$\left[\gamma_{\theta z}^{(e)}(r,\theta,z,t)\right]^{(m)}=\sum_{i=1}^{n_d}\left(D_z\,\phi_i^{(e)}\right)\left(v_i^{(e)}\right)^{(m)}+(1/r)\sum_{i=1}^{n_d}\left(\phi_i^{(e)}\right)\left(w_{i,\theta}^{(e)}\right)^{(m)} \quad (13)$$

$$\left[\gamma_{r\theta}^{(e)}(r,\theta,z,t)\right]^{(m)}=(1/r)\sum_{i=1}^{n_d}\left(\phi_i^{(e)}\right)\left(u_{i,\theta}^{(e)}\right)^{(m)}+\sum_{i=1}^{n_d}\left(D_r\,\phi_i^{(e)}\right)\left(v_i^{(e)}\right)^{(m)}-(1/r)\sum_{i=1}^{n_d}\left(\phi_i^{(e)}\right)\left(v_i^{(e)}\right)^{(m)} \quad (14)$$

where the commas denote partial differentiation with respect to the suffix variables, and $D_r\phi_i^{(e)}=\partial\phi_i^{(e)}/\partial r$, $D_z\phi_i^{(e)}=\partial\phi_i^{(e)}/\partial z$.

2.2 The Hamilton principle

The Hamilton principle is used to derive the motion equations of the FG annular plate, and the corresponding functional (I_R) of the plate is written in the form of

$$I_R=\int_{t_1}^{t_2}L\;dt \quad (15)$$

where L represents the Lagrange energy functional, $L=T-\Pi_R$, in which T and Π_R denote the kinetic energy and RMVT-based potential energy functionals, respectively, and they are given as

$$T=\int_{-h/2}^{h/2}\int_0^{2\pi}\int_{R_1}^{R_2}\left\{(\rho/2)\left[\left(\partial u_r/\partial t\right)^2+\left(\partial u_\theta/\partial t\right)^2+\left(\partial u_z/\partial t\right)^2\right]\right\}r\,dr\,d\theta\,dz \quad (16)$$

$$\begin{aligned}\Pi_R=&\int_{-h/2}^{h/2}\int_0^{2\pi}\int_{R_1}^{R_2}\left[\sigma_r\,\varepsilon_r+\sigma_\theta\,\varepsilon_\theta+\sigma_z\,\varepsilon_z+\tau_{rz}\,\gamma_{rz}+\tau_{\theta z}\,\gamma_{\theta z}+\tau_{r\theta}\,\gamma_{r\theta}-B\left(\sigma_{ij}\right)\right]r\,dr\,d\theta\,dz\\&-\int_{-h/2}^{h/2}\int_{\Gamma_\sigma}\left(\bar{t}_k\,u_k\right)d\Gamma\,dz-\int_{-h/2}^{h/2}\int_{\Gamma_u}\left[(u_k-\bar{u}_k)\,t_k\right]d\Gamma\,dz\end{aligned} \quad (17)$$

where ρ is the mass density of the plate considered, Γ_σ and Γ_u denote the portions of the edge boundary, in which the surface traction and displacement components (i.e., $\bar{t}_k$ and $\bar{u}_k$ (k = r, θ and z)) are prescribed, respectively, and $B(\sigma_{ij})$ is the complementary energy density function.

Substituting the kinematic and kinetic assumptions, given in Eqs. (2)-(4) and (5)-(7), respectively, in Eqs. (16) and (17) and performing the first-order variation of I_R lead to the following form

$$\delta I_R=\delta\int_{t_1}^{t_2}L\;dt=\delta\int_{t_1}^{t_2}\left(T-\Pi_R\right)dt \quad (18)$$

$$\delta\int_{t_1}^{t_2}T\;dt=\int_{t_1}^{t_2}\sum_{m=1}^{N_l}\sum_{e=1}^{N_e}\left\{\int_0^{2\pi}\iint_{A_e}\left[-\rho\left(\delta\mathbf{u}^{(e)}\right)^T\left(\partial^2\mathbf{u}^{(e)}/\partial t^2\right)-\rho\left(\delta\mathbf{w}^{(e)}\right)^T\left(\partial^2\mathbf{w}^{(e)}/\partial t^2\right)\right]^{(m)}r\,dA_e\,d\theta\right\}dt \quad (19)$$

$$\begin{aligned}\delta\int_{t_1}^{t_2}\Pi_R\,dt=\int_{t_1}^{t_2}\Bigg\{&\sum_{m=1}^{N_l}\sum_{e=1}^{N_e}\left\{\int_0^{2\pi}\iint_{A_e}\left\{\left(\delta\boldsymbol{\varepsilon}_p^{(e)}\right)^T\boldsymbol{\sigma}_p^{(e)}\right.\right.\\&+\left(\delta\boldsymbol{\varepsilon}_s^{(e)}\right)^T\boldsymbol{\sigma}_s^{(e)}+\delta\varepsilon_z^{(e)}\,\sigma_z^{(e)}+\left(\delta\boldsymbol{\sigma}_s^{(e)}\right)^T\left(\boldsymbol{\varepsilon}_s^{(e)}-\mathbf{S}^{(e)}\boldsymbol{\sigma}_s^{(e)}\right)\\&\left.\left.+\delta\sigma_z^{(e)}\left[\varepsilon_z^{(e)}-\left(c_{33}^{(e)}\right)^{-1}\sigma_z^{(e)}+\left(\mathbf{Q}_z^{(e)}\right)^T\boldsymbol{\varepsilon}_p^{(e)}\right]\right\}^{(m)}r\,dA_e\,d\theta\right\}dt\end{aligned} \quad (20)$$

where the symbols N_e and A_e denote the number of annular prisms in each individual layer and the cross-sectional area of a typical annular prism, respectively; the superscript T stands for the transposition of the matrices or vectors, and

$\boldsymbol{\varepsilon}_p^{(e)}=\left[\varepsilon_r^{(e)}\quad\varepsilon_\theta^{(e)}\quad\gamma_{r\theta}^{(e)}\right]^T=\mathbf{B}_1^{(e)}\,\mathbf{u}^{(e)}$,

$\boldsymbol{\sigma}_p^{(e)}=\left[\sigma_r^{(e)}\quad\sigma_\theta^{(e)}\quad\tau_{r\theta}^{(e)}\right]^T=\mathbf{Q}_p^{(e)}\,\mathbf{B}_1^{(e)}\,\mathbf{u}^{(e)}+\mathbf{Q}_z^{(e)}\,\mathbf{B}_2^{(e)}\,\boldsymbol{\sigma}^{(e)}$,

$\boldsymbol{\varepsilon}_s^{(e)}=\left[\gamma_{rz}^{(e)}\quad\gamma_{\theta z}^{(e)}\right]^T=\mathbf{B}_3^{(e)}\,\mathbf{u}^{(e)}+\mathbf{B}_4^{(e)}\,\mathbf{w}^{(e)}$,

$\boldsymbol{\sigma}_s^{(e)}=\left[\tau_{rz}^{(e)}\quad\tau_{\theta z}^{(e)}\right]^T=\mathbf{B}_5^{(e)}\,\boldsymbol{\tau}^{(e)}$, $\varepsilon_z^{(e)}=\mathbf{B}_6^{(e)}\,\mathbf{w}^{(e)}$,

$\sigma_z^{(e)}=\mathbf{B}_2^{(e)}\,\boldsymbol{\sigma}^{(e)}$, $\mathbf{u}^{(e)}=\begin{bmatrix}u_i^{(e)}\\v_i^{(e)}\end{bmatrix}$, $\mathbf{w}^{(e)}=\left[w_i^{(e)}\right]$, $\boldsymbol{\tau}^{(e)}=\begin{bmatrix}\left(\tau_{13}^{(e)}\right)_i\\\left(\tau_{23}^{(e)}\right)_i\end{bmatrix}$,

$\boldsymbol{\sigma}^{(e)}=\left[\left(\sigma_3^{(e)}\right)_i\right]$, $\mathbf{S}^{(e)}=\begin{bmatrix}\left(1/c_{55}^{(e)}\right)&0\\0&\left(1/c_{44}^{(e)}\right)\end{bmatrix}$,

$\mathbf{Q}_p^{(e)}=\begin{bmatrix}Q_{11}^{(e)}&Q_{12}^{(e)}&0\\Q_{12}^{(e)}&Q_{22}^{(e)}&0\\0&0&Q_{66}^{(e)}\end{bmatrix}$,

$\mathbf{Q}_z^{(e)}=\begin{bmatrix}Q_{13}^{(e)}\\Q_{23}^{(e)}\\0\end{bmatrix}$, $\mathbf{B}_1^{(e)}=\begin{bmatrix}\left(D_r\,\phi_i^{(e)}\right)&0\\(1/r)\,\phi_i^{(e)}&(1/r)\phi_i^{(e)}\partial_\theta\\(1/r)\,\phi_i^{(e)}\partial_\theta&\left(D_r\,\phi_i^{(e)}\right)-(1/r)\,\phi_i^{(e)}\end{bmatrix}$,

$\mathbf{B}_2^{(e)}=\left[\phi_i^{(e)}\right]$, $\mathbf{B}_3^{(e)}=\begin{bmatrix}\left(D_z\,\phi_i^{(e)}\right)&0\\0&\left(D_z\,\phi_i^{(e)}\right)\end{bmatrix}$, $\mathbf{B}_4^{(e)}=\begin{bmatrix}\left(D_r\,\phi_i^{(e)}\right)\\(1/r)\left(\phi_i^{(e)}\right)\partial_\theta\end{bmatrix}$,

$\mathbf{B}_5^{(e)}=\begin{bmatrix}\left(\phi_i^{(e)}\right)&0\\0&\left(\phi_i^{(e)}\right)\end{bmatrix}$, $\mathbf{B}_6^{(e)}=\left[\left(D_z\,\phi_i^{(e)}\right)\right]$, in which i = 1, 2, …, n_d;

$Q_{kl}^{(e)}=c_{kl}^{(e)}-(c_{k3}^{(e)}\,c_{l3}^{(e)}/c_{33}^{(e)})$ (k, l = 1 and 2),

$Q_{k3}^{(e)}=c_{k3}^{(e)}/c_{33}^{(e)}$ (k = 1 and 2), $Q_{66}^{(e)}=c_{66}^{(e)}$.

2.3 Motion equations

The free vibration behavior of a multilayered FG annular plate with combinations of free, clamped, and simply-supported boundary edges is studied in the following illustrative examples, in which the material properties are considered to obey an exponential function distribution varying doubly exponentially through the radial-thickness surface, while they are independent of the circumferential direction.

Nine different boundary conditions considered in this work are given as follows:

For clamped-clamped (C-C) supports,

$$u_r^{(e)}=u_\theta^{(e)}=u_z^{(e)}=0 \quad \text{at } r=R_1 \text{ and } R_2. \quad (21)$$

For clamped-simply supported (C-S) supports,

$$u_r^{(e)}=u_\theta^{(e)}=u_z^{(e)}=0 \quad \text{at } r=R_1, \quad (22a)$$

$$u_\theta^{(e)}=u_z^{(e)}=\sigma_r^{(e)}=0 \quad \text{at } r=R_2. \quad (22b)$$

For clamped-free (C-F) supports,

$$u_r^{(e)}=u_\theta^{(e)}=u_z^{(e)}=0 \quad \text{at } r=R_1, \quad (23a)$$

$$\sigma_r^{(e)}=\tau_{r\theta}^{(e)}=\tau_{rz}^{(e)}=0 \quad \text{at } r=R_2. \quad (23b)$$

For simply supported-clamped (S-C) supports,

$$u_\theta^{(e)} = u_z^{(e)} = \sigma_r^{(e)} = 0 \quad \text{at } r = R_1, \tag{24a}$$

$$u_r^{(e)} = u_\theta^{(e)} = u_z^{(e)} = 0 \quad \text{at } r = R_2. \tag{24b}$$

For simply supported-simply supported (S-S) supports,

$$u_\theta^{(e)} = u_z^{(e)} = \sigma_r^{(e)} = 0 \quad \text{at } r = R_1 \text{ and } r = R_2. \tag{25}$$

For simply supported-free (S-F) supports,

$$u_\theta^{(e)} = u_z^{(e)} = \sigma_r^{(e)} = 0 \quad \text{at } r = R_1, \tag{26a}$$

$$\sigma_r^{(e)} = \tau_{r\theta}^{(e)} = \tau_{rz}^{(e)} = 0 \quad \text{at } r = R_2. \tag{26b}$$

For free-clamped (F-C) supports,

$$\sigma_r^{(e)} = \tau_{r\theta}^{(e)} = \tau_{rz}^{(e)} = 0 \quad \text{at } r = R_1, \tag{27a}$$

$$u_r^{(e)} = u_\theta^{(e)} = u_z^{(e)} = 0 \quad \text{at } r = R_2. \tag{27b}$$

For free-simply supported (F-S) supports,

$$\sigma_r^{(e)} = \tau_{r\theta}^{(e)} = \tau_{rz}^{(e)} = 0 \quad \text{at } r = R_1, \tag{28a}$$

$$u_\theta^{(e)} = u_z^{(e)} = \sigma_r^{(e)} = 0 \quad \text{at } r = R_2. \tag{28b}$$

For free-free (F-F) supports,

$$\sigma_r^{(e)} = \tau_{r\theta}^{(e)} = \tau_{rz}^{(e)} = 0 \quad \text{at } r = R_1 \text{ and } r = R_2. \tag{29}$$

This formulation can also be used for the analysis of multi-layered FG circular plates. In that case, the edge conditions at $r = R_2$ for the free, simply-supported and clamped edges will remain the same as those mentioned above, while the edge conditions at $r = R_1$ should be replaced with the continuity conditions at $r = 0$, which are given as

$$u_r^{(e)} = u_\theta^{(e)} = \tau_{rz}^{(e)} = 0 \quad \text{at} \quad r = 0. \tag{30}$$

In this formulation, the primary field variables of each individual annular prism, which are given in Eqs. (2)-(7), are further expanded as the single Fourier series in the circumferential coordinate and assigned the harmonic function in the time domain, and they are rewritten as

$$\left(u_r^{(e)}\right)^{(m)} = \sum_{\hat{n}=0}^{\infty}\sum_{j=1}^{n_d} \left(\phi_j^{(e)}\right)\left(u_{\hat{n}}^{(e)}\right)_j^{(m)} \cos\hat{n}\theta \; e^{i\omega t} \tag{31}$$

$$\left(u_\theta^{(e)}\right)^{(m)} = \sum_{\hat{n}=0}^{\infty}\sum_{j=1}^{n_d} \left(\phi_j^{(e)}\right)\left(v_{\hat{n}}^{(e)}\right)_j^{(m)} \sin\hat{n}\theta \; e^{i\omega t} \tag{32}$$

$$\left(u_z^{(e)}\right)^{(m)} = \sum_{\hat{n}=0}^{\infty}\sum_{j=1}^{n_d} \left(\phi_j^{(e)}\right)\left(w_{\hat{n}}^{(e)}\right)_j^{(m)} \cos\hat{n}\theta \; e^{i\omega t} \tag{33}$$

$$\left(\tau_{rz}^{(e)}\right)^{(m)} = \sum_{\hat{n}=0}^{\infty}\sum_{j=1}^{n_d} \left(\phi_j^{(e)}\right)\left(\tau_{13\hat{n}}^{(e)}\right)_j^{(m)} \cos\hat{n}\theta \; e^{i\omega t} \tag{34}$$

$$\left(\tau_{\theta z}^{(e)}\right)^{(m)} = \sum_{\hat{n}=0}^{\infty}\sum_{j=1}^{n_d} \left(\phi_j^{(e)}\right)\left(\tau_{23\hat{n}}^{(e)}\right)_j^{(m)} \sin\hat{n}\theta \; e^{i\omega t} \tag{35}$$

$$\left(\sigma_z^{(e)}\right)^{(m)} = \sum_{\hat{n}=0}^{\infty}\sum_{j=1}^{n_d} \left(\phi_j^{(e)}\right)\left(\sigma_{3\hat{n}}^{(e)}\right)_j^{(m)} \cos\hat{n}\theta \; e^{i\omega t} \tag{36}$$

where $\hat{n}$ denotes the half-wave number of a typical vibration mode, the value of which is either a positive integer or zero, and ω represents the natural frequencies of the plate.

Introducing the kinetic and kinematic models of the FAPMs (Eqs. (31)-(36)) and the corresponding boundary conditions at the edges, given in Eqs. (21)-(29), and applying the Halmiton principle (i.e., $\delta I_R = 0$), we thus obtain the motion equations of the multi-layered FG annular plate as follows:

$$\sum_{m=1}^{N_l}\sum_{e=1}^{N_e}\left\{\begin{bmatrix} k_{11}^{(e)} & k_{12}^{(e)} & 0 & k_{14}^{(e)} & 0 & k_{16}^{(e)} \\ k_{21}^{(e)} & k_{22}^{(e)} & 0 & 0 & k_{25}^{(e)} & k_{26}^{(e)} \\ 0 & 0 & 0 & k_{34}^{(e)} & k_{35}^{(e)} & k_{36}^{(e)} \\ k_{41}^{(e)} & 0 & k_{43}^{(e)} & k_{44}^{(e)} & 0 & 0 \\ 0 & k_{52}^{(e)} & k_{53}^{(e)} & 0 & k_{55}^{(e)} & 0 \\ k_{61}^{(e)} & k_{62}^{(e)} & k_{63}^{(e)} & 0 & 0 & k_{66}^{(e)} \end{bmatrix} - \omega^2 \begin{bmatrix} m_{11}^{(e)} & 0 & 0 & 0 & 0 & 0 \\ 0 & m_{22}^{(e)} & 0 & 0 & 0 & 0 \\ 0 & 0 & m_{33}^{(e)} & 0 & 0 & 0 \\ 0 & 0 & 0 & 0 & 0 & 0 \\ 0 & 0 & 0 & 0 & 0 & 0 \\ 0 & 0 & 0 & 0 & 0 & 0 \end{bmatrix}^{(m)}\right\} \begin{bmatrix} \left(u_{\hat{n}}^{(e)}\right)_j \\ \left(v_{\hat{n}}^{(e)}\right)_j \\ \left(w_{\hat{n}}^{(e)}\right)_j \\ \left(\tau_{13\hat{n}}^{(e)}\right)_j \\ \left(\tau_{23\hat{n}}^{(e)}\right)_j \\ \left(\sigma_{3\hat{n}}^{(e)}\right)_j \end{bmatrix}^{(m)} = \sum_{m=1}^{N_l}\sum_{e=1}^{N_e}\begin{bmatrix} 0 \\ 0 \\ 0 \\ 0 \\ 0 \\ 0 \end{bmatrix}^{(m)} \tag{37}$$

where $k_{ij}^{(e)}\left(\phi_i^{(e)}, \phi_j^{(e)}\right) = k_{ji}^{(e)}\left(\phi_j^{(e)}, \phi_i^{(e)}\right)$; $k_{ij}^{(e)}$ can refer to Wu and Yu [55], and $m_{11}^{(e)} = m_{22}^{(e)} = m_{33}^{(e)} = \iint_{A_e} \rho r \, \varphi_i^{(e)} \varphi_j^{(e)} \, dA_e$, where $i, j = 1\text{-}n_d$.

By imposing the continuity conditions of each node's nodal primary variables (i.e., the nodal displacement and transverse stress components) at the nodal lines between adjacent prisms, the local stiffness and mass matrices of each prism in Eq. (37) can be assembled as their corresponding global stiffness and mass matrices for the FG annular plate, and Eq. (37) can be rewritten as follows:

$$\left\{\begin{bmatrix} \mathbf{K}_{11} & \mathbf{K}_{12} & \mathbf{0} & \mathbf{K}_{14} & \mathbf{0} & \mathbf{K}_{16} \\ \mathbf{K}_{21} & \mathbf{K}_{22} & \mathbf{0} & \mathbf{0} & \mathbf{K}_{25} & \mathbf{K}_{26} \\ \mathbf{0} & \mathbf{0} & \mathbf{0} & \mathbf{K}_{34} & \mathbf{K}_{35} & \mathbf{K}_{36} \\ \mathbf{K}_{41} & \mathbf{0} & \mathbf{K}_{43} & \mathbf{K}_{44} & \mathbf{0} & \mathbf{0} \\ \mathbf{0} & \mathbf{K}_{52} & \mathbf{K}_{53} & \mathbf{0} & \mathbf{K}_{55} & \mathbf{0} \\ \mathbf{K}_{61} & \mathbf{K}_{62} & \mathbf{K}_{63} & \mathbf{0} & \mathbf{0} & \mathbf{K}_{66} \end{bmatrix} - \left(\omega^2\right)\begin{bmatrix} \mathbf{M}_{11} & \mathbf{0} & \mathbf{0} & \mathbf{0} & \mathbf{0} & \mathbf{0} \\ \mathbf{0} & \mathbf{M}_{22} & \mathbf{0} & \mathbf{0} & \mathbf{0} & \mathbf{0} \\ \mathbf{0} & \mathbf{0} & \mathbf{M}_{33} & \mathbf{0} & \mathbf{0} & \mathbf{0} \\ \mathbf{0} & \mathbf{0} & \mathbf{0} & \mathbf{0} & \mathbf{0} & \mathbf{0} \\ \mathbf{0} & \mathbf{0} & \mathbf{0} & \mathbf{0} & \mathbf{0} & \mathbf{0} \\ \mathbf{0} & \mathbf{0} & \mathbf{0} & \mathbf{0} & \mathbf{0} & \mathbf{0} \end{bmatrix}\right\}\begin{bmatrix} \mathbf{u} \\ \mathbf{v} \\ \mathbf{w} \\ \boldsymbol{\tau}_{13} \\ \boldsymbol{\tau}_{23} \\ \boldsymbol{\sigma}_3 \end{bmatrix} = \begin{bmatrix} \mathbf{0} \\ \mathbf{0} \\ \mathbf{0} \\ \mathbf{0} \\ \mathbf{0} \\ \mathbf{0} \end{bmatrix}. \tag{38}$$

Eq. (38) represents a standard eigenvalue problem, and a nontrivial solution of this exists if the determinant of the coefficient matrix vanishes. The natural frequencies of the multi-layered FG annular plate for a set of fixed values $(\hat{n})$ and their corresponding mode shapes can thus be obtained.

Table 1. Convergence of T3, T6 and T10 FAPM solutions for the first five frequency parameters of fully-clamped, one-directional exponential function-type FG circular plates with different vibration modes.

n	Theories	Ω_1	Ω_2	Ω_3	Ω_4	Ω_5
0	Current T3 (16x4)	0.1005	0.3335	0.4113	0.6329	0.6986
	Current T3 (32x4)	0.0994	0.3281	0.4101	0.6220	0.6946
	Current T3 (32x8)	0.0965	0.3188	0.4101	0.6038	0.6945
	Current T3 (64x16)	0.0954	0.3149	0.4097	0.5953	0.6933
	Current T6 (8x4)	0.0959	0.3180	0.4097	0.6047	0.6952
	Current T6 (16x4)	0.0953	0.3146	0.4096	0.5952	0.6934
	Current T6 (32x4)	0.0951	0.3139	0.4096	0.5933	0.6930
	Current T6 (32x8)	0.0951	0.3137	0.4096	0.5927	0.6930
	Current T10 (8x4)	0.0953	0.3143	0.4096	0.5938	0.6935
	Current T10 (16x4)	0.0951	0.3137	0.4096	0.5927	0.6930
	Current T10 (32x4)	0.0951	0.3135	0.4096	0.5924	0.6929
	Kermani et al. [47]	0.095	0.314	0.410	0.593	0.693
	Nie and Zhong [45]	0.096	NA	NA	NA	NA
1	Current T3 (16x4)	0.2026	0.4158	0.4740	0.6196	0.7782
	Current T3 (32x4)	0.1981	0.4044	0.4678	0.6046	0.7793
	Current T3 (32x8)	0.1923	0.4044	0.4547	0.6047	0.7569
	Current T3 (64x16)	0.1889	0.3917	0.4482	0.5980	0.7465
	Current T6 (8x4)	0.1925	0.4078	0.4531	0.6059	0.7574
	Current T6 (16x4)	0.1892	0.3998	0.4482	0.5994	0.7466
	Current T6 (32x4)	0.1879	0.3939	0.4463	0.5954	0.7437
	Current T6 (32x8)	0.1877	0.3940	0.4459	0.5954	0.7426
	Current T10 (8x4)	0.1886	0.4001	0.4460	0.5993	0.7409
	Current T10 (16x4)	0.1877	0.3941	0.4457	0.5955	0.7422
	Current T10 (32x8)	0.1870	0.3895	0.4450	0.5925	0.7418
	Kermani et al. [47]	0.187	0.390	0.445	0.593	0.746
	Nie and Zhong [45]	0.186	NA	NA	NA	NA
2	Current T3 (16x4)	0.2924	0.5585	0.5993	0.7493	0.9238
	Current T3 (32x4)	0.2889	0.5543	0.5906	0.7411	0.9195
	Current T3 (32x8)	0.2832	0.5542	0.5774	0.7411	0.8966
	Current T3 (64x16)	0.2807	0.5530	0.5711	0.7389	0.8851
	Current T6 (8x4)	0.2829	0.5544	0.5787	0.7403	0.9055
	Current T6 (16x4)	0.2807	0.5530	0.5713	0.7384	0.8864
	Current T6 (32x4)	0.2801	0.5527	0.5697	0.7383	0.8827
	Current T6 (32x8)	0.2800	0.5526	0.5693	0.7382	0.8819
	Current T10 (8x4)	0.2805	0.5530	0.5703	0.7383	0.8849
	Current T10 (16x4)	0.2800	0.5526	0.5692	0.7382	0.8815
	Current T10 (32x4)	0.2799	0.5525	0.5690	0.7382	0.8811
	Kermani et al. [47]	0.280	0.553	0.569	0.738	0.882
	Nie and Zhong [45]	0.277	NA	NA	NA	NA

3. Illustrative examples

3.1 One-directional exponential function-type FG circular plates

For comparison purposes, the authors examine the free vibration behavior of a one-directional exponential function-type FG circular plate with clamped boundary conditions, in which the continuity conditions at the center of the circular plate are used as mentioned in Eq. (30). The problem was previously investigated by Nie and Zhong [45] and Kermani et al. [47] using the SSDQ method, and the corresponding solutions are thus used to validate the accuracy and convergence rate of solutions obtained using the current T3, T6 and T10 IFAPMs.

The material properties of the one-directional FG circular plate are assumed to obey an exponential function distribution through the thickness direction, as follows:

$$c_{ij}(z) = c_{ij}^0\, e^{\kappa_{ez}[0.5+(z/h)]} \tag{39a}$$

$$\rho(z) = \rho_0\, e^{\kappa_{ez}[0.5+(z/h)]} \tag{39b}$$

where κ_{ez} stands for the material-property gradient index in the thickness directions. ρ_0 denotes the mass density at the bottom surface of the circular plates. c_{ij}^0 (i, j = 1-6) are the elastic coefficients at the bottom surface of the circular plate, and are given as follows:

$$\mathbf{C}_0 = \begin{bmatrix} c_{11}^0 & c_{12}^0 & c_{12}^0 & 0 & 0 & 0 \\ c_{12}^0 & c_{11}^0 & c_{12}^0 & 0 & 0 & 0 \\ c_{12}^0 & c_{12}^0 & c_{11}^0 & 0 & 0 & 0 \\ 0 & 0 & 0 & \left(c_{11}^0 - c_{12}^0\right)/2 & 0 & 0 \\ 0 & 0 & 0 & 0 & \left(c_{11}^0 - c_{12}^0\right)/2 & 0 \\ 0 & 0 & 0 & 0 & 0 & \left(c_{11}^0 - c_{12}^0\right)/2 \end{bmatrix} \tag{40}$$

Table 2. Convergence of T3, T6 and T10 FAPM solutions for the lowest frequency parameters of fully-clamped, one-directional exponential function-type FG circular plates with different values of aspect ratios and material property gradient indices κ_{ez}.

h/R_2	Theories	$\kappa_{ez}=0$	$\kappa_{ez}=1$	$\kappa_{ez}=2$	$\kappa_{ez}=3$	$\kappa_{ez}=4$	$\kappa_{ez}=5$
0.2	Current T3 (16x4)	0.1030	0.1005	0.0947	0.0868	0.0784	0.0705
	Current T3 (32x4)	0.1016	0.0994	0.0938	0.0861	0.0779	0.0701
	Current T3 (32x8)	0.0987	0.0965	0.0907	0.0827	0.0740	0.0657
	Current T3 (64x16)	0.0976	0.0954	0.0896	0.0816	0.0728	0.0644
	Current T6 (8x4)	0.0981	0.0959	0.0900	0.0819	0.0730	0.0644
	Current T6 (16x4)	0.0975	0.0953	0.0895	0.0814	0.0725	0.0640
	Current T6 (32x4)	0.0973	0.0951	0.0893	0.0812	0.0724	0.0639
	Current T6 (32x8)	0.0973	0.0951	0.0893	0.0812	0.0724	0.0639
	Current T10 (8x4)	0.0975	0.0953	0.0895	0.0814	0.0725	0.0640
	Current T10 (16x4)	0.0973	0.0951	0.0893	0.0812	0.0724	0.0639
	Current T10 (32x4)	0.0972	0.0951	0.0893	0.0812	0.0724	0.0639
	Nie and Zhong [45]	0.098	0.096	0.090	0.082	0.073	0.064
0.4	Current T3 (16x4)	0.3315	0.3253	0.3104	0.2899	0.2675	0.2458
	Current T3 (32x4)	0.3293	0.3236	0.3091	0.2890	0.2669	0.2454
	Current T3 (32x8)	0.3210	0.3152	0.2997	0.2780	0.2540	0.2303
	Current T3 (64x16)	0.3181	0.3124	0.2967	0.2746	0.2500	0.2258
	Current T6 (8x4)	0.3190	0.3130	0.2971	0.2747	0.2498	0.2252
	Current T6 (16x4)	0.3179	0.3120	0.2962	0.2739	0.2490	0.2244
	Current T6 (32x4)	0.3175	0.3117	0.2959	0.2737	0.2488	0.2243
	Current T6 (32x8)	0.3172	0.3115	0.2957	0.2735	0.2487	0.2242
	Current T10 (8x4)	0.3177	0.3119	0.2961	0.2738	0.2489	0.2243
	Current T10 (16x4)	0.3173	0.3115	0.2958	0.2736	0.2487	0.2242
	Current T10 (32x4)	0.3171	0.3114	0.2957	0.2735	0.2487	0.2241
	Nie and Zhong [45]	0.319	0.313	0.298	0.275	0.250	0.225

in which $\mathbf{C}_0$ is the elastic coefficient matrix at the bottom surface of the circular plate, the relevant coefficients c_{ij}^0 of which can be obtained using the corresponding Young's modulus E_0 and Poisson's ratio υ_0, as well as $c_{11}^0 = E_0(1-\upsilon_0)/[(1+\upsilon_0)(1-2\upsilon_0)]$, $c_{12}^0 = c_{11}^0\,\upsilon_0/(1-\upsilon_0)$. In this paper, the ceramic material is used as the reference material, the material properties of which are $E_0 = 380$ GPa, $\upsilon_0 = 0.3$ and $\rho_0 = 3800$ kg/m^3 [45, 47].

Table 1 shows the convergence studies for the current T3, T6 and T10 FAPM solutions of the first five frequency parameters of the FG circular plate with clamped boundary conditions and different vibration modes, in which a dimensionless frequency parameter Ω is defined as $\Omega = \omega h\sqrt{\rho_0/c_{11}^0}$. The material-property gradient index κ_{ez} is taken to be $\kappa_{ez} = 1$, and the aspect ratios of the circular plate are taken to be $h/R_2 = 0.2$ and $h = 0.2$ m. Table 2 shows the convergence studies for the current T3, T6 and T10 FAPM solutions for the lowest frequency parameters of the FG circular plate with clamped boundary conditions, different aspect ratios, and different material-property gradient indices values. In these two tables, the uniform meshes on the nodal surface (i.e., the radial-thickness surface) are taken to be ($n_r \times n_z$) = (16x4), (32x4), (32x8) and (64x16) for the T3 FAPM, ($n_r \times n_z$) = (8x4), (16x4), (32x4) and (32x8) for the T6 FAPM, and ($n_r \times n_z$) = (8x4), (16x4) and (32x4) for the T10 FAPM, in which n_r and n_z are the total numbers of annular prisms used in the radial and thickness directions, respectively.

It can be seen in Tables 1 and 2 that the current FAPM solutions converge rapidly. The convergent solutions for T3, T6 and T10 FAPM are obtained when meshes ($n_r \times n_z$) = (64x16), (32x8) and (32x4) are used, respectively. These convergent solutions are shown to be in excellent agreement with the 3D SSDQ solutions obtained by Kermani et al. [47] and Nie and Zhong [45]. The performance of these FAPMs are T10 > T6 > T3, in which the symbol ">" represents more accurate solutions and a fast convergence rate, such that the T6 with a uniform (32x8) mesh and the T10 with a uniform (32x4) mesh are recommended for the following parametric study with regard to the free vibration analysis of the bi-directional exponential function-type FG annular plates with nine different boundary conditions. Results also show the frequency parameters decrease when the material-property gradient index (κ_{ez}) becomes greater and the plate thickness-to-radius ratio (h/R_2) becomes lesser, which represents the gross stiffness-to-mass ratio of the FG circular plate becomes softer.

3.2 Bi-directional exponential function-type FG annular plates

The free vibration behavior of a bi-directional exponential function-type FG annular plate with various boundary conditions is investigated in this section. The material properties of the FG annular plate are assumed to obey a bi-directional exponential function distribution over the radial-thickness surface. They are given as follows:

$$c_{ij}(r,\, z) = c_{ij}^0\, e^{\kappa_{ez}[0.5+(z/h)]}\, e^{\kappa_{er}(r/R_2)}, \tag{41a}$$

$$\rho(r,\, z) = \rho_0\, e^{\kappa_{ez}[0.5+(z/h)]}\, e^{\kappa_{er}(r/R_2)}, \tag{41b}$$

Table 3. Convergent solutions of T6 and T10 FAPMs for the first five frequency parameters of bi-directional exponential function-type FG annular plates with different boundary conditions.

BCs	Theories	Ω_1	Ω_2	Ω_3	Ω_4	Ω_5
C-C	Current T6 (32x8)	0.2578	0.4877	0.5696	0.7827	0.8817
	Current T10 (32x4)	0.2576	0.4877	0.5691	0.7825	0.8817
C-S	Current T6 (32x8)	0.1726	0.3558	0.4877	0.5046	0.8817
	Current T10 (32x4)	0.1725	0.3557	0.4877	0.5043	0.8817
C-F	Current T6 (32x8)	0.0404	0.0492	0.2279	0.3555	0.5854
	Current T10 (32x4)	0.0404	0.0492	0.2277	0.3555	0.5850
S-C	Current T6 (32x8)	0.2283	0.4877	0.5451	0.6344	0.8817
	Current T10 (32x4)	0.2282	0.4877	0.5449	0.6343	0.8817
S-S	Current T6 (32x8)	0.1453	0.2983	0.4757	0.4877	0.8670
	Current T10 (32x4)	0.1453	0.2983	0.4757	0.4877	0.8668
S-F	Current T6 (32x8)	0.0276	0.0492	0.2000	0.2980	0.5574
	Current T10 (32x4)	0.0276	0.0492	0.2000	0.2980	0.5573
F-C	Current T6 (32x8)	0.1129	0.3534	0.4559	0.6329	0.6866
	Current T10 (32x4)	0.1129	0.3532	0.4559	0.6329	0.6863
F-S	Current T6 (32x8)	0.0485	0.2823	0.2977	0.4559	0.6257
	Current T10 (32x4)	0.0485	0.2823	0.2977	0.4559	0.6256
F-F	Current T6 (32x8)	0.0788	0.2974	0.3490	0.5855	0.7066
	Current T10 (32x4)	0.0788	0.2974	0.3490	0.5855	0.7065

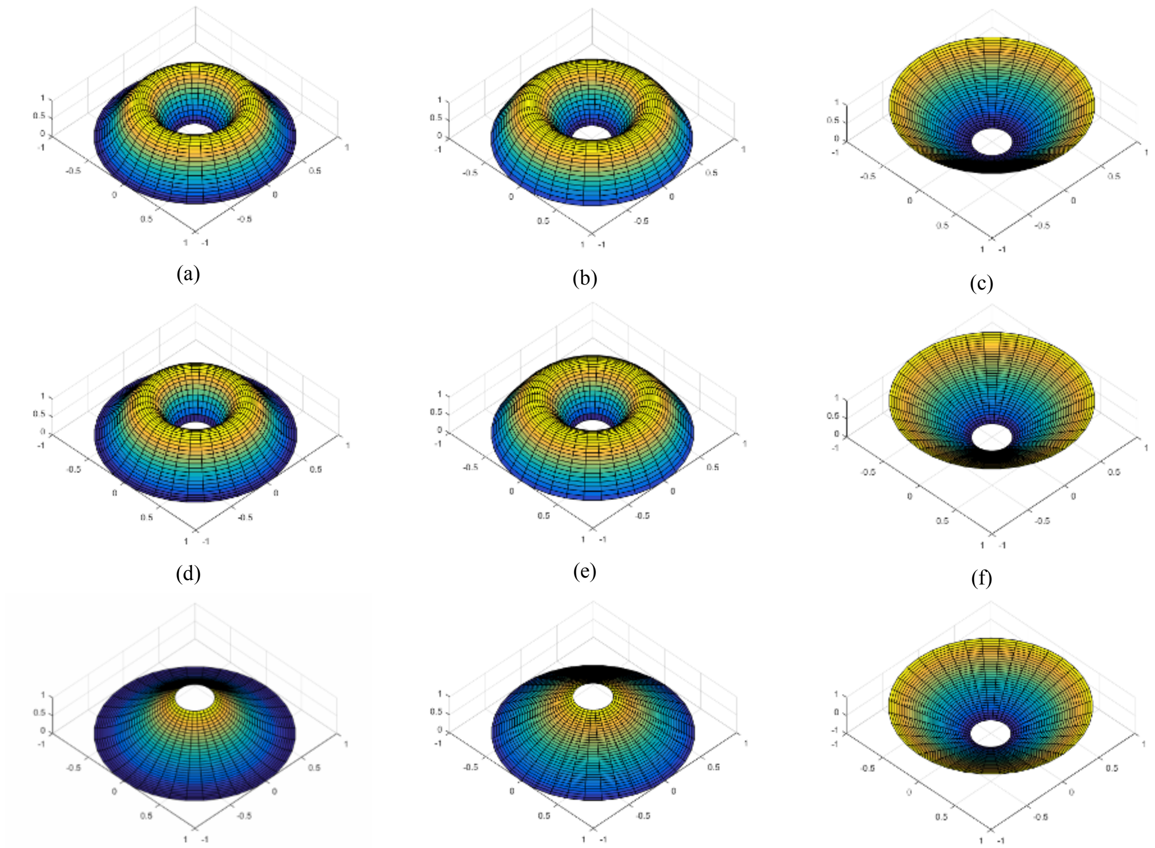
(a) (b) (c) (d) (e) (f) (g) (h) (i)

Fig. 3. The mode shapes of the displacement component u_z corresponding to the lowest frequency parameter of the bi-directional exponential function-type FG annular plate with (a) C-C; (b) C-S; (c) C-F; (d) S-C; (e) S-S; (f) S-F; (g) F-C; (h) F-S; (i) F-F boundary conditions.

where κ_{er} stands for the material-property gradient index in the radial directions.

A dimensionless frequency parameter Ω is defined as having the same form as that used in the numerical example 3.1.

Table 3 shows the convergent solutions of T6 and T10

Table 4. Convergent solutions of T6 and T10 FAPMs for the lowest frequency parameters of simply-supported, bi-directional exponential function-type FG annular plates with different values of the inner radius-to-outer radius ratios.

Theories	$R_1/R_2 = 0.05$	$R_1/R_2 = 0.1$	$R_1/R_2 = 0.3$	$R_1/R_2 = 0.5$	$R_1/R_2 = 0.8$
Current T6 (32x8)	0.1119	0.1207	0.1825	0.2333	0.1963
Current T10 (32x4)	0.1118	0.1207	0.1825	0.2333	0.1963

Table 5. Convergent solutions of T6 and T10 FAPMs for the lowest frequency parameters of simply-supported, bi-directional exponential function-type FG annular plates with different values of the material-property gradient indices κ_{ez} and κ_{er} .

	$k_{ez} = 1$		$k_{ez} = 2$		$k_{ez} = 3$	
$k_{ez} = 1$	Current T6 (32x8)	0.1453	Current T6 (32x8)	0.1386	Current T6 (32x8)	0.1310
	Current T10 (32x4)	0.1453	Current T10 (32x4)	0.1386	Current T10 (32x4)	0.1310
$k_{ez} = 2$	Current T6 (32x8)	0.1367	Current T6 (32x8)	0.1305	Current T6 (32x8)	0.1236
	Current T10 (32x4)	0.1367	Current T10 (32x4)	0.1305	Current T10 (32x4)	0.1235
$k_{ez} = 3$	Current T6 (32x8)	0.1248	Current T6 (32x8)	0.1193	Current T6 (32x8)	0.1130
	Current T10 (32x4)	0.1247	Current T10 (32x4)	0.1193	Current T10 (32x4)	0.1130

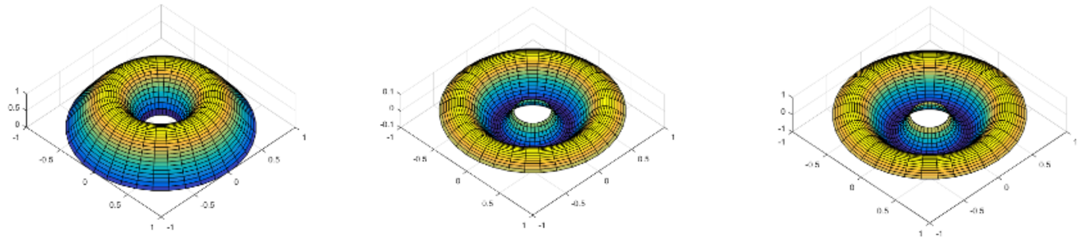

(a) (b) (c)

Fig. 4. The mode shapes of the displacement component u_z corresponding to the first three frequency parameters of the simply-supported, bi-directional exponential function-type FG annular plate (a) Ω_1 ; (b) Ω_2 ; (c) Ω_3 , in which $\hat{n} = 0$.

FAPMs for the first five frequency parameters of the bi-directional exponential function-type FG annular plates with nine different boundary conditions, which are the CC, CS, CF, SC, SS, SF, FC, FS and FF boundary conditions, where $\kappa_{er} = \kappa_{ez} = 1$; $h/R_2 = 0.2$; $R_1/R_2 = 0.2$ and $R_2 = 1$ m, and $\hat{n} = 0$, which is the axisymmetric mode. It can be seen in Table 3 that the solutions of frequency parameters of the plate obtained using the T6 FAPM with the mesh (32x8) and the T10 FAPM with the mesh (32x4) are closely agree with each other, and that the effects of different boundary conditions on the frequency parameters of the annular plate are significant. It is noted that the lowest frequency parameters of the annular plates do not always occur at $\hat{n}$ = 0 when the plates under a free edge condition. For example, the lowest frequency parameters occur at $\hat{n} = 2$ for the FF boundary conditions, and at $\hat{n} = 1$ for the CF and SF boundary conditions, which are asymmetric vibration modes, while $\hat{n} = 0$, which is the axisymmetric vibration mode, for the others. The magnitude order of the lowest frequency parameters of the annular plates for different boundary conditions is CC > SC > CS > SS > FC > FS for the axisymmetric vibration mode cases, which reflects the magnitude order with regard to the gross stiffness of the annular plates with different boundary conditions. This observation is also supported by the results of Liu and Lee [56] and Zhou et al. [57], in which the free vibration behavior of a single-layered isotropic annular plate with different boundary conditions was examined.

Fig. 3 shows the mode shapes of the displacement u_z at the mid-surface of the bi-directional exponential function-type FG axisymmetric annular plates with nine different boundary conditions, CC, CS, CF, SC, SS, SF, FC, FS and FF, in which $h/R_2 = 0.1$; $R_1/R_2 = 0.2$ and $R_2 = 1$ m; $\kappa_{er} = \kappa_{ez} = 1$ and $\hat{n} = 0$. As expected, the results show the axisymmetric behavior to occur in the circumferential direction for the plates with assorted boundary conditions.

Fig. 4 shows the mode shapes of the displacement u_z on the mid-surface of the bi-directional exponential function-type FG annular plates with SS boundary conditions for the vibration modes corresponding to the first three lowest frequency parameters, i.e., Ω_i $(i = 1-3)$, in which h/R_2 = 0.1; R_1/R_2 = 0.2 and R_2 = 1 m; $\kappa_{er} = \kappa_{ez} = 2$ and $\hat{n} = 0$. Again, axisymmetric behavior in the circumferential direction for these mode shapes of the displacement component u_z is observed, while there are no remarkable variations similar to those of trigonometric functions with a series of half wave numbers in the radial direction because there are variable coefficients appearing in the motion equations in the radial direction, which make it impossible to represent the vibration behavior of the annular plate as the simple harmonic vibration mode.

Table 4 shows the convergent solutions of T6 and T10 FAPMs for the lowest frequency parameters of simply-supported, bi-directional exponential function-type FG annular plates with different values of inner radius-to-outer radius ratios, in which h/R_2 = 0.2, R_2 = 1 m, $\kappa_{er} = \kappa_{ez} = 1$, $\hat{n} = 0$ and R_1/R_2 = 0.05, 0.1, 0.3, 0.5 and 0.8. It can be seen in Table 4 that the convergent solutions of T6 FAPM with the (32x8) mesh are exactly the same as those of T10 FAPM with the (32x4) mesh. The frequency parameters initially increase when the R_1/R_2 ratio change from 0.05 to 0.5, and then they will decrease when the R_1/R_2 ratio becomes greater.

Table 5 shows the convergent solutions of T6 and T10 FAPMs for the lowest frequency parameters of simply-supported, bi-directional exponential function-type FG annular plates with different values of the material-property gradient indices κ_{er} and κ_{ez}, in which h/R_2 = 0.2, R_1/R_2 = 0.2, R_2 = 1 m, and $\hat{n} = 0$. It can be seen in Table 5 that the frequency parameters decrease when the values of κ_{er} and κ_{ez} become greater. Results also show the frequency parameter in the case of $(\kappa_{er},\ \kappa_{ez}) = (3,\ 1)$ is 9.84 % lesser than that that in the case of $(\kappa_{er},\ \kappa_{ez}) = (1,\ 1)$, and the frequency parameter in the case of $(\kappa_{er},\ \kappa_{ez}) = (1,\ 3)$ is 14.1 % lesser than that that in the case of $(\kappa_{er},\ \kappa_{ez}) = (1,\ 1)$. The effect of κ_{ez} on the frequency parameter of the FG annular plate is more significant than the effect of κ_{er}.

4. Concluding remarks

Within the framework of 3D elasticity theory, the authors develop a weak-form formulation of various RMVT-based FAPMs to examine the free vibration behavior of bi-directional exponential function-type FG thick annular plates with nine different boundary conditions. Implementation of these FAPMs shows that the current FAPM solutions converge rapidly and that their convergent solutions are in excellent agreement with the 3D SSDQ solutions available in the literature. The performance of assorted FAPMs is T10 > T6 > T3, in which the symbol ">" represents more accurate results and a rapid convergence rate, and the current T6 and T10 FAPMs with the (32x8) and (32x4) meshes, respectively, are recommended for the analysis of typical bi-directional FG thick annular and circular plates.

In the numerical examples, the results show that the effects of different boundary conditions on the frequency parameters of the bi-directional FG annular plates are significant. The frequency parameters decrease when the material-property gradient index becomes greater and the plate becomes thinner, which represents the gross stiffness-to-mass ratio of the FG circular plate becomes softer. In addition, the effect of κ_{ez} on the frequency parameter of the FG annular plate is more significant than the effect of κ_{er}. Because accurate solutions for the issue discussed herein are rare in the literature, these convergent solutions obtained using the FAPMs can provide a reference for assessing the performance of other numerical methods.

References

[1] M. Koizumi, Concept of FGM, *Ceramic Trans*., 34 (1993) 3-10.

[2] M. Koizumi, FGM activities in Japan, *Compos. Part B-Eng.,* 28 (1-2) (1997) 1-4.

[3] J. N. Reddy, C. M. Wang and S. Kitipornchai, Axisymmetric bending of functionally graded circular and annular plates, *Eur. J. Mech. A/Solids,* 18 (2) (1999) 185-199.

[4] K. Swaminathan, D. T. Naveenkumar, A. M. Zenkour and E. Carrera, Stress, vibration and buckling analyses of FGM plates-A state-of-the art review, *Compos. Struct*., 120 (2015) 10-31.

[5] E. Carrera, S. Brischetto and A. Robaldo, Variable kinematic model for the analysis of functionally graded material plates, *AIAA J*., 46 (1) (2008) 194-203.

[6] M. Cinefra, S. Belouettar, M. Soave and E. Carrera, Variable kinematic models applied to free-vibration analysis of functionally graded material shells, *Eur. J. Mech. A/Solids,* 29 (6) (2010) 1078-1087.

[7] D. K. Jha, T. Kant and R. K. Singh, A critical review of recent research on functionally graded plates, *Compos. Struct.,* 96 (2013) 833-849.

[8] F. Tornabene and S. Brischetto, 3D capability of refined GDQ models for the bending analysis of composite and sandwich plates, spherical and doubly-curved shells, *Thin-Walled Struct*., 129 (2018) 94-124.

[9] C. P. Wu, K. H. Chiu and Y. M. Wang, A review on the three-dimensional analytical approaches of multilayered and functionally graded piezoelectric plates and shells, *CMC-Comput. Mater. Continua,* 8 (2) (2008) 93-132.

[10] C. P. Wu and Y. C. Liu, A review of semi-analytical numerical methods for laminated composite and multilayered functionally graded elastic/piezoelectric plates and shells, *Compos. Struct*., 147 (2016) 1-15.

[11] Y. Ootao, Y. Tanigawa and O. Ishimaru, Optimization of material composition of functionally graded plate for thermal stress relaxation using a genetic algorithm, *J. Therm. Stresses,* 23 (3) (2000) 257-271.

[12] S. Ding and C. P. Wu, Optimization of material composition to minimize the thermal stresses induced in FGM plates with temperature-dependent material properties, *Int. J. Mech. Mater. Des.,* 14 (4) (2018) 527-549.

[13] O. S. Hussein and S. B. Mulani, Optimization of in-plane functionally graded panels for buckling strength: Unstiffened, stiffened panels, and panels with cutouts, *Thin-Walled Struct*., 122 (2018) 173-181.

[14] L. F. Qian and R. C. Batra, Design of bidirectional functionally graded plate for optimal natural frequencies, *J. Sound Vib.,* 280 (2005) 415-424.

[15] Y. Kumar and R. Lal, Prediction of frequencies of free axisymmetric vibration of two-directional functionally graded annular plates on Winkler foundation, *Eur. J. Mech. A/Solids,* 42 (2013) 219-228.

[16] R. Lal and N. Ahlawat, Buckling and vibrations of two-

directional functionally graded circular plates subjected to hydrostatic in-plane force, *J. Vib. Control,* 23 (13) (2017) 2111-2127.

[17] F. Tornabene, E. Viola and D. J. Inman, 2-D differential quadrature solution for vibration analysis of functionally graded conical, cylindrical shell and annular plate structures, *J. Sound Vib*., 328 (3) (2009) 259-290.

[18] Z. Su, G. Jin, S. Shi, T. Ye and X. Jia, A unified solution for vibration analysis of functionally graded cylindrical, conical shells and annular plates with general boundary conditions, *Int. J. Mech. Sci*., 80 (2014) 62-80.

[19] Q. Wang, D. Shi, Q. Liang and X. Shi, A unified solution for vibration analysis of functionally graded circular, annular and sector plates with general boundary conditions, *Compos. Part B-Eng.,* 88 (2016) 264-294.

[20] F. Tornabene, Free vibration analysis of functionally graded conical, cylindrical shell and annular plate structures with a four-parameter power-law distribution, *Comput. Methods Appl. Mech. Engrg*., 198 (37-40) (2009) 2911-2935.

[21] M. H. Amini, M. Soleimani, A. Altafi and A. Rastgoo, Effects of geometric nonlinearity on free and forced vibration analysis of moderately thick annular functionally graded plate, *Mech. Adv. Mater. Struct*., 20 (9) (2013) 709-720.

[22] A. R. Saidi, A. Rasouli and S. Sahraee, Axisymmetric bending and buckling analysis of thick functionally graded circular plates using unconstrained third-order shear deformation plate theory, *Compos. Struct.,* 89 (2009) 110-119.

[23] M. Talha and B. N. Singh, Static response and free vibration analysis of FGM plates using higher order shear deformation theory, *Appl. Math. Modell*., 34 (12) (2010) 3991-4011.

[24] S. Hosseini-Hashemi, M. Es'haghi, H. R. D. Taher and M. Fadaie, Exact closed-form frequency equations for thick circular plates using a third-order shear deformation theory, *J. Sound Vib*., 329 (16) (2010) 3382-3396.

[25] S. Sahraee and A. R. Saidi, Axisymmetric bending analysis of thick functionally graded circular plates using fourth-order shear deformation theory, *Eur. J. Mech. A/Solids,* 28 (5) (2009) 974-984.

[26] R. C. Batra, Higher-order shear and normal deformable theory for functionally graded incompressible linear elastic plates, *Thin-Walled Struct.,* 45 (12) (2007) 974-982.

[27] A. J. M. Ferreira, R. C. Batra, C. M. C. Roque, L. F. Qian and R. M. N. Jorge, Natural frequencies of functionally graded plates by a meshless method, *Compos. Struct.,* 75 (2006) 593-600.

[28] R. Lal and R. Rani, On radially symmetric vibrations of non-uniform annular sandwich plates, *Thin-Walled Struct*., 94 (2015) 562-576.

[29] P. Malekzadeh and N. S. Hamzehkolaei, A 3D discrete layer-differential quadrature free vibration of multilayered FG annular plates in thermal environment, *Mech. Adv. Mater. Struct*., 20 (4) (2013) 316-330.

[30] E. Carrera, Theories and finite elements for multilayered, anisotropic, composite plates and shells, *Arch. Comput. Meth. Engng.,* 9 (2) (2002) 87-140.

[31] K. Mercan, A. K. Baltacioglu and Ö. Civalek, Free vibration of laminated and FGM/CNT composites annular thick plates with shear deformation by discrete singular convolution method, *Compos. Struct.,* 186 (2018) 139-153.

[32] X. Shi, C. Li, F. Wang and F. Wei, A unified formulation for free transverse vibration analysis of orthotropic plates of revolution with general boundary conditions, *Mech. Adv. Mater. Struct.,* 25 (2) (2018) 87-99.

[33] T. J. R. Hughes, J. A. Cottrell and Y. Bazilevs, Isogeometric analysis: CAD, finite elements, NURBS, exact geometry and mesh refinement, *Comput. Methods Appl. Mech. Eng*., 194 (39-41) (2005) 4135-4195.

[34] J. A. Cottrell, T. J. R. Hughes and Y. Bazilevs, *Isogeometric Analysis: Toward Integration of CAD and FEA,* Chichesrer, United Kindom: John Wiley & Sons (2009).

[35] X. Qin, G. Jin, M. Chen and S. Yin, Free in-plane vibration analysis of circular, annular, and sector plates using isogeometric approach, *Shock Vib.,* 4314761 (2018).

[36] Q. X. Lieu, S. Lee, J. Kang and J. Lee, Bending and free vibration analyses of in-plane bi-directional functionally graded plates with variable thickness using isogeometric analysis, *Compos. Struct.,* 192 (2018) 434-451.

[37] J. So and A. W. Leissa, Three-dimensional vibrations of thick circular and annular plates, *J. Sound Vib.,* 209 (1) (1998) 15-41.

[38] J. H. Kang and A. W. Leissa, Three-dimensional vibrations of thick, linearly tapered, annular plates, *J. Sound Vib.,* 217 (5) (1998) 927-944.

[39] K. M. Liew and B. Yang, Three-dimensional elasticity solutions for free vibrations of circular plates: A polynomials-Ritz analysis, *Comput. Methods Appl. Mech. Eng*., 175 (1-2) (1999) 189-201.

[40] K. M. Liew and B. Yang, Elasticity solutions for free vibrations of annular plates from three-dimensional analysis, *Int. J. Solids Struct*., 37 (52) (2000) 7689-7702.

[41] D. Zhou, F. T. K. Au, Y. K. Cheung and S. H. Lo, Three-dimensional vibration analysis of circular and annular plates via the Chebyshev-Ritz method, *Int. J. Solids Struct*., 40 (12) (2003) 3089-3105.

[42] D. Zhou, S. H. Lo, F. T. K. Au and Y. K. Cheung, Three-dimensional free vibration of thick circular plates on Pasternak foundation, *J. Sound Vib*., 292 (3-5) (2006) 726-741.

[43] P. Shi and C. Y. Dong, Vibration analysis of functionally graded annular plates with mixed boundary conditions in thermal environment, *J. Sound Vib*., 331 (15) (2012) 3649-3662.

[44] C. Y. Dong, Three-dimensional free vibration analysis of functionally graded annular plates using the Chebyshev-Ritz method, *Mater. Des*., 29 (8) (2008) 1518-1525.

[45] G. Nie and Z. Zhong, Dynamic analysis of multi-directional functionally graded annular plates, *Appl. Math. Modell*., 34 (3) (2010) 608-616.

[46] G. J. Nie and Z. Zhong, Vibration analysis of functionally graded annular sectorial plates with simply supported radial edges, *Compos. Struct*., 84 (2) (2008) 167-176.

[47] I. D. Kermani, M. Ghayour and H. R. Mirdamadi, Free vibration analysis of multi-directional functionally graded circular and annular plates, *J. Mech. Sci. Technol*., 26 (11) (2012) 3399-3410.
[48] P. Malekzadeh, S. A. Shahpari and H. R. Ziaee, Three-dimensional free vibration of thick functionally graded annular plates in thermal environment, *J. Sound Vib*., 329 (4) (2010) 425-442.
[49] S. S. Vel and R. C. Batra, Three-dimensional exact solution for the vibration of functionally graded rectangular plates, *J. Sound Vib.,* 272 (3-5) (2004) 703-730.
[50] J. Zhao, Y. Zhang, K. Choe, X. Qu, A. Wang and Q. Wang, Three-dimensional exact solution for the free vibration of thick functionally graded annular sector plates with arbitrary boundary conditions, *Compos. Part B,* 159 (2019) 418-436.
[51] E. Carrera, Historical review of zig-zag theories for multilayered plates and shells, *Appl. Mech. Rev*., 56 (3) (2003) 287-308.
[52] E. Carrera, Assessment of theories for free vibration analysis of homogeneous and multilayered plates, *Shock Vib*., 11 (3-4) (2004) 261-270.
[53] C. P. Wu and H. Y. Li, An RMVT-based finite rectangular prism method for the 3D analysis of sandwich FGM plates with various boundary conditions, *CMC-Comput. Mater. Continua.,* 34 (1) (2013) 27-62.
[54] C. P. Wu and H. Y. Li, RMVT-based finite cylindrical prism methods for multilayered functionally graded circular hollow cylinders with various boundary conditions, *Compos. Struct*., 100 (2013) 592-608.
[55] C. P. Wu and L. T. Yu, Quasi-3D static analysis of two-directional functionally graded circular plates, *Steel Compos. Struct.,* 27 (2018) 789-801.
[56] C. F. Liu and Y. T. Lee, Finite element analysis of three-dimensional vibrations of thick circular and annular plates, *J. Sound Vib*., 233 (1) (2000) 63-80.
[57] D. Zhou, F. T. K. Au, Y. K. Cheung and S. H. Lo, Three-dimensional vibration analysis of circular and annular plates via the Chebyshev-Ritz method, *Int. J. Solids Struct*., 40 (12) (2003) 3089-3105.

Chih-Ping Wu obtained his Ph.D. degree from the Engineering Mechanics, Ohio State University, USA, in 1988. Since then, he worked as an Associate Professor at the Department of Civil Engineering (CE), National Cheng Kung University (NCKU), Taiwan. In 1993 and 2003, he was promoted to be the Full Professor and Distinguished Professor at NCKU, respectively. From 2003 to 2006, he served as the Head of the CE Department, NCKU. He majored in the research areas including FGM plates/shells, nonlocal continuum mechanics, computational mechanics, finite element methods, meshless methods, perturbation methods, and three-dimensional elasticity/piezoelectricity.